Copyright WILEY-VCH Verlag GmbH & Co. KGaA, 69469 Weinheim, Germany, 2015.

ADVANCED ENERGY MATERIALS

Supporting Information

for *Adv. Energy Mater.,* DOI: 10.1002/aenm.201500096

A Tale of Two Sites: On Defining the Carrier Concentration in Garnet-Based Ionic Conductors for Advanced Li Batteries

*Travis Thompson, Asma Sharafi, Michelle D. Johannes, Ashfia Huq, Jan L. Allen, Jeff Wolfenstine, and Jeff Sakamoto**

DOI: 10.1002/aenm.201500096

Article type: Full paper

A Tale of Two Sites: On Defining the Carrier Concentration in Garnet-based Ionic Conductors for Advanced Li Batteries

Travis Thompson, Asma Sharafi, Michelle D. Johannes, Ashfia Huq, Jan L. Allen, Jeff Wolfenstine, and Jeff Sakamoto*

Travis. Thompson, Asma Sharafi, Jeff Sakamoto
Department of Mechanical Engineering
University of Michigan
2350 Hayward Ave, GG Brown Laboratory, Ann Arbor, MI 48109
Email: jeffsaka@umich.edu

Michelle D. Johannes
Center for Computational Materials Science
Naval Research Laboratory, Anacostia, VA

Ashfia Huq
Spallation Neutron Source
Oak Ridge National Laboratory, Oak Ridge TN

Jan L. Allen, Jeff Wolfenstine
RDRL-SED-C
Army Research Laboratory
2800 Powder Mill Road, Adelphi, MD 20783

Keywords: solid electrolyte, garnet, neutron diffraction, ionic conductivity, battery

Copyright WILEY-VCH Verlag GmbH & Co. KGaA, 69469 Weinheim, Germany, 2013.

Supporting Information

A Tale of Two Sites: On Defining the Carrier Concentration in Garnet-based Ionic Conductors for Advanced Li Batteries
Travis Thompson, Asma Sharafi, Michelle D. Johannes, Ashfia Huq, Jan L. Allen, Jeff Wolfenstine, and Jeff Sakamoto *

EIS model

Electrochemical Impedance Spectroscopy (EIS) was performed as a function of temperature. Nyquist plots of EIS data are often modeled using the brick-layer model.[1,2] In the brick-layer model, it is common to add in parallel combinations of a resistor and a capacitor to represent each semi-circle observed in the Nyquist plot of the impedance spectra. Thus, three parallel combinations are often used, one for the bulk, a second for the grain boundaries, and a third for the electrolyte/electrode interface. This, however, is not a physical representation of the system. For this work, the EIS data were modeled using a modified equivalent circuit proposed by Huggins.[2] Although this model is similar to the conventional brick-layer model, it specifically treats the arrangement of capacitive elements differently. Instead, Huggins placed the capacitive element for bulk transport in parallel with all the other elements in the model since it is a better representation of the physical arrangement of the system. For a detailed development of the model, the reader is directed to reference.[2]

Figure 3 shows a representative Nyquist plot of the EIS data for composition $Li_{6.5}La_3Zr_{1.5}Ta_{0.5}O_{12}$ at room temperature, the equivalent circuit, the modeled impedance response, and a simulation to frequencies in the gigahertz regime. The salient features are labeled with their characteristic frequencies. For this study, the model developed by Huggins was modified in three ways. First, the leg of the circuit which corresponds to electronic leakage through the electrolyte was removed since DC measurements have confirmed the electronic portion to be negligible and a low frequency tail was always observed in the impedance spectra. Second, a mass transport element was added in parallel to the capacitor which corresponds to the blocking electrodes since there is some solubility of Li in Pt. This non-ideal blocking behavior of the inert electrodes has been observed in most of the reports of EIS data for LLZO in the literature, regardless of the noble metal used.[3-7] Huggins mentions the use of a Warburg type

element for this but we chose an element corresponding to anomalous diffusion since our electrodes are thin sputtered Pt films. For full discussion of the impedance response of anomalous diffusive type elements, the reader is directed to the following reference.[8]

Lastly, the capacitors in the Huggins model were replaced with constant phase elements (CPEs) to account for any dispersion to the time constants. The complex impedance response of a single CPE is given by:

$$Z(\omega) = \frac{1}{Q(j\omega)^{\alpha}}$$

The ideality of the CPE is represented by the coefficient α. When α is zero, the element is behaving as a resistor and when α is 1 it is behaving as an ideal capacitor. The values for the ideality coefficient α were allowed to freely refine and settled to values near or exactly 1 after convergence. The values of Q should be on the order of ~10^{-12} Fcm^{-2} for the bulk and ~10^{-9} Fcm^{-2} for the grain boundaries.[1, 2] Excellent agreement with the expected CPE Q values for these physical processes was observed.

It should be noted that because of the high Li conduction in these samples, especially in the x = 0.5 Ta composition, not all of the temperature points could be modeled due to the maximum EIS perturbation frequency of 7 MHz. It can be seen in Figure 3 that even at room temperature, the characteristic frequency for the bulk response does not occur until >12 MHz. As such, the Arrhenius plot of the bulk conductivities (Figure S1) explicitly excludes points at elevated temperature which we could not model with certainty.

The room temperature total conductivity, shown in Table 1, is a sum of the bulk and grain boundary conductivities obtained from the modeling. The total impedance response was normalized to the bulk geometry before modeling was performed. Thus, the grain boundary process appears to have a higher conductivity compared to the bulk. This is, however, just an

artifact of the geometric normalization and if the grain boundary geometry were to be estimated from other means, it is expected that the grain boundary process would be more resistive. The fact that the grain boundary contribution is low is evidence that the grains are well connected and that results for the bulk response can be treated with more certainty since the impedance response primarily corresponds to that process.

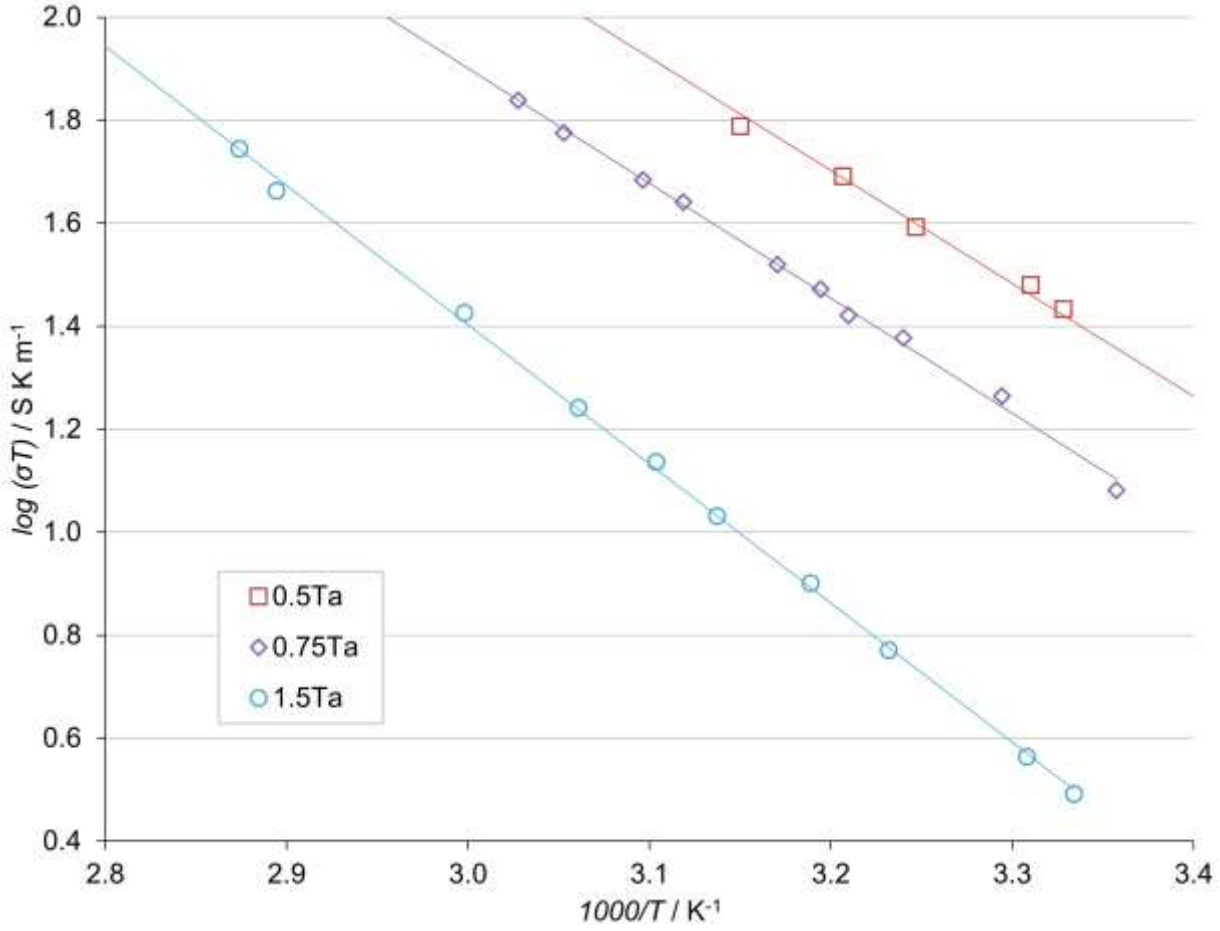

Figure S1. Arrhenius plot of the bulk, not total, conductivity of our compositional series as determined form the equivalent circuit modeling.

Development of the structural model

In cubic LLZO there are two Li coordination environments; tetrahedral and octahedral coordination with oxygen. There are two ways to define the site of the octahedrally coordinated

Li. The first is with a single symmetric Wyckoff position 48g. The second is with a displaced Wyckoff positions referred to as 96h sites. The 96h position represents the splitting of the proposed 48g site into two off-center 96h sites each oppositely adjacent to the 48g site, where only one of 96h sites can be filled at any one time due to Li-Li columbic repulsion. Earlier structural models used the 48g position or a combination of the 48g and 96h, however, subsequent studies have pointed to the 96h position as being the correct description of the octahedrally coordinated Li.[9-13] In order to compare structural models together, an octahedral occupancy for the Li has been defined as $Li_{\text{octahedral}} = 2 * Occ_{Li96h} + Occ_{Li48g}$. In this work, where only the 96h site was considered, the octahedral Li occupancy was calculated by $Li_{\text{octahedral}} = 2 * Occ_{Li96h} + 0$. As seen in Table 2, S1, S2, modeling the experimental data with the octahedrally coordinated Li described only by the 96h site resulted in excellent fits with low χ^2 values in the range of 3 – 6, and R_{wp} values as low as ~2.5 being achieved. This indicated that the structural results could be treated with more certainty.

Since the purpose of this study was to probe the Li environment directly with a technique which is sensitive to it (i.e. neutron diffraction) without the need for assumptions regarding the Li content, the Li stoichiometry was not assumed and allowed to freely refine in the structural model without the imposition of charge balance. This is a similar to the approach used in the structural model of Goodenough *et al.* [5] In contrast, the model of Logeat *et al.* assumed the nominal Li content to maintain charge balance.[11] Since it was not the intent of this work to make assumptions regarding the stoichiometry of the system, it was deemed reasonable to allow the Li sites to freely refine at the expense of possible charge imbalance. Charge imbalance of -0.88, -0.80, and -0.76 for the Ta = 0.5, 0.75, and 1.5 compositions respectively was observed in our work but oxygen vacancies could easily account for the difference seen and have, in fact,

been proposed, but not discussed, in the literature previously by Goodenough *et al.*[5] The possibility of oxygen vacancies was explored in the structural model of this work, however, the oxygen site occupancy refined to an unphysical result without a significant increase in the goodness-of-fit to the experimental data. Therefore, the oxygen content was left fixed at the nominal for the determination of the Li site occupancy. The presence of a second crystal defect, besides what is purposefully introduced by the dopant, could be another, uncontrolled variable. Since the Li content is the conventional parameter used to discuss Li-ion conducting garnets, the influence of oxygen defects on the Li-ion transport in garnets deserves more investigation, if these defects are indeed present. Since the presence and role of other charge compensating defects, which could alter the Li content, is not resolved, the nominal Li content is used to discuss the results shown in Figure 5A and Figure 5B.

Diffraction patterns

Included below are all the neutron and synchrotron X-ray diffraction patterns. Two neutron histograms, one X-ray histogram, and a magnified region of the X-ray histogram are included for each composition. Even though the neutron beamline used for the diffraction presented here is high resolution, the synchrotron X-ray source has approximately an order of magnitude higher resolving power. It was only in the synchrotron X-ray diffraction that it became apparent that more than one cubic phase is present for the Ta = 0.5 and 0.75 compositions. This is the first observance of this in Ta doped LLZO but has been observed before for Al doped LLZO.[14] However, the Ta = 1.5 composition was apparently a single cubic phase. This shows that the solid solution formed between the Zr and Ta end members is not continuous but forms at discrete compositions. However, it should be noted that since the two cubic phases are not resolvable by table-top X-ray diffraction, let alone high resolution neutron

diffraction, that the differences in the two cubic phases present are minimal. This is supported by our structural refinements of the synchrotron diffraction data.

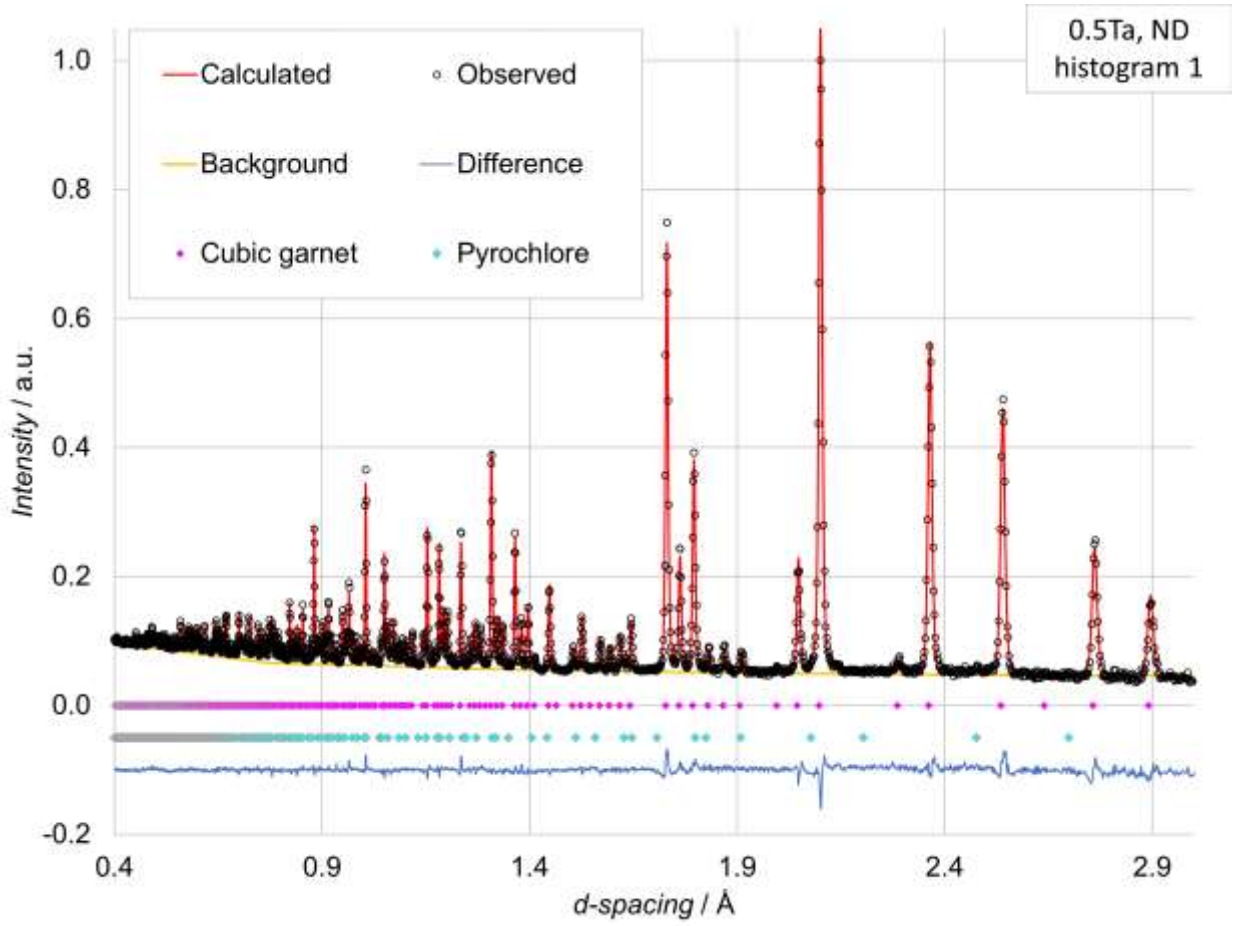

Figure S2. Refinement of neutron diffraction data after convergence for the sample with composition of $Li_{6.5}La_3Zr_{1.5}Ta_{0.5}O_{12}$.

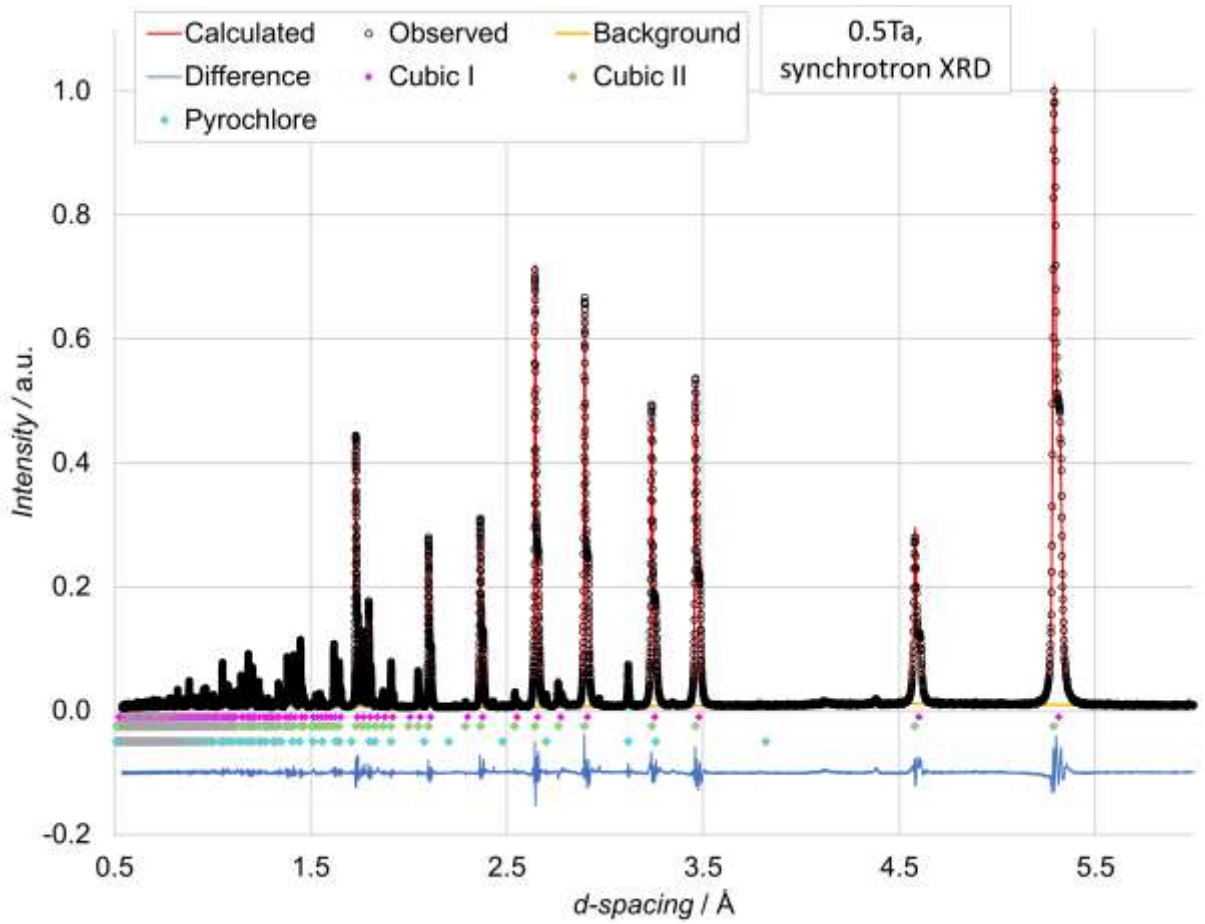

Figure S3. Refinement of synchrotron X-ray diffraction data after convergence for the sample with composition of $Li_{6.5}La_3Zr_{1.5}Ta_{0.5}O_{12}$.

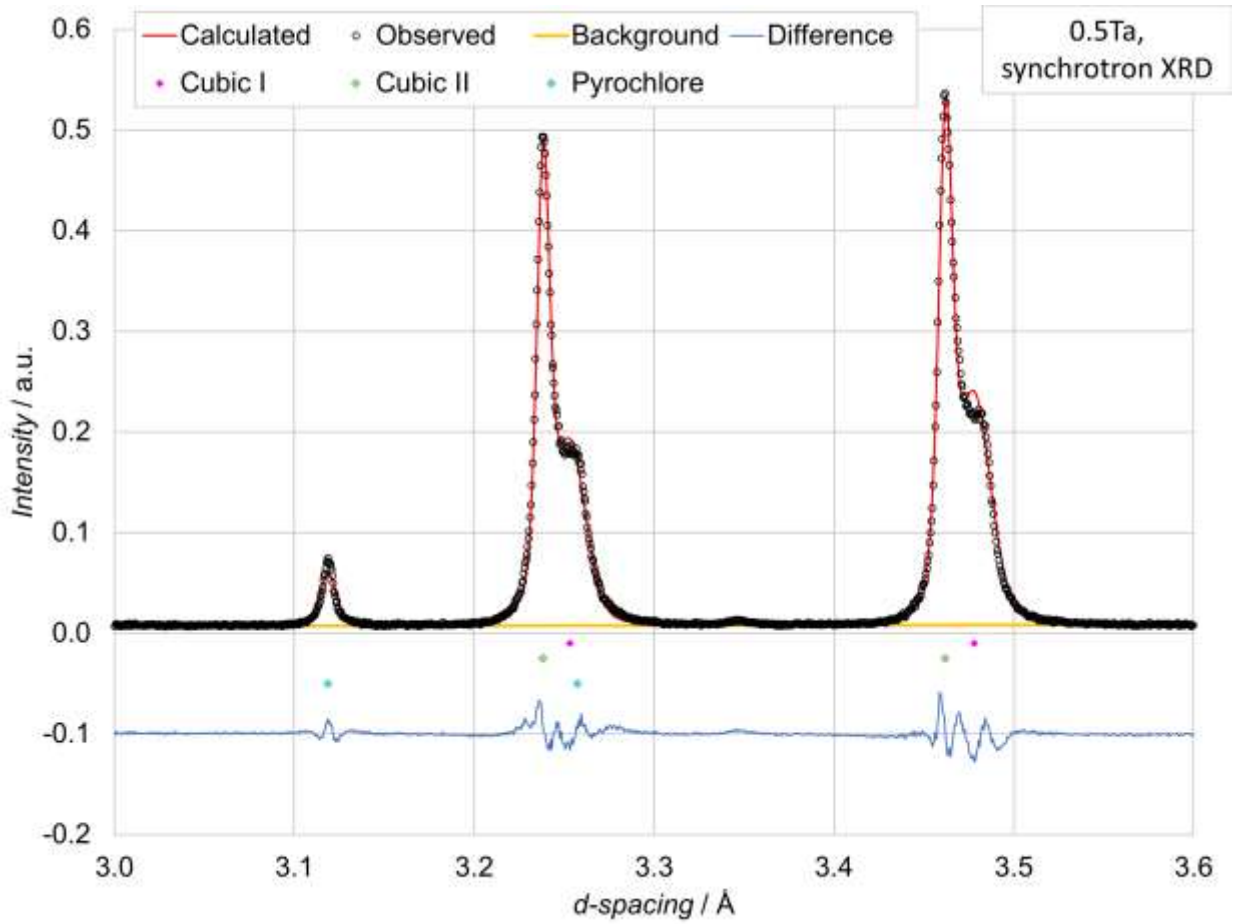

Figure S4. Magnified region of the refinement of synchrotron x-ray diffraction data after convergence for the sample with composition of $Li_{6.5}La_3Zr_{1.5}Ta_{0.5}O_{12}$ highlighting the two cubic phases observed.

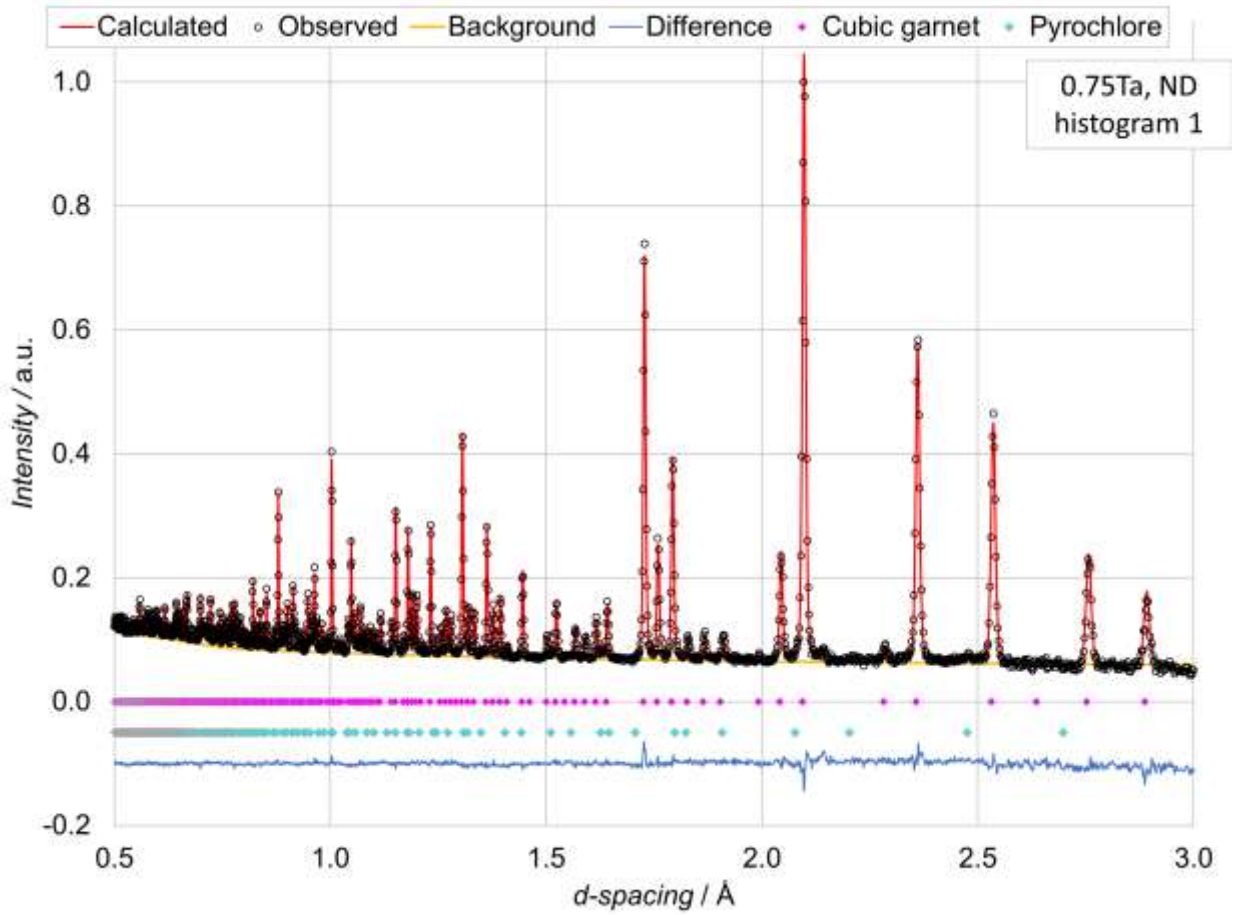

Figure S5. Refinement of neutron diffraction data after convergence for the sample with composition of $Li_{6.25}La_3Zr_{1.25}Ta_{0.75}O_{12}$.

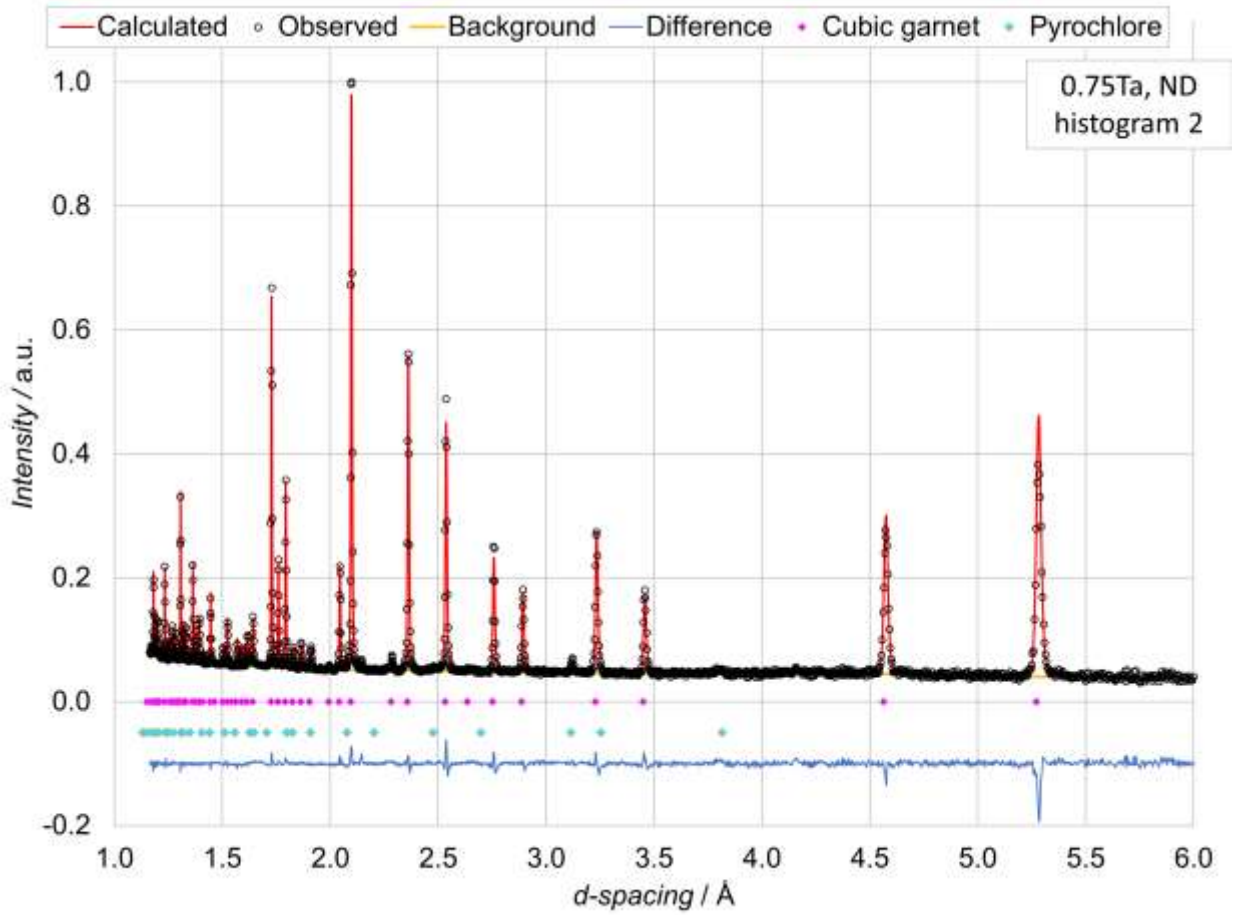

Figure S6. Refinement of neutron diffraction data after convergence for the sample with composition of $Li_{6.25}La_3Zr_{1.25}Ta_{0.75}O_{12}$.

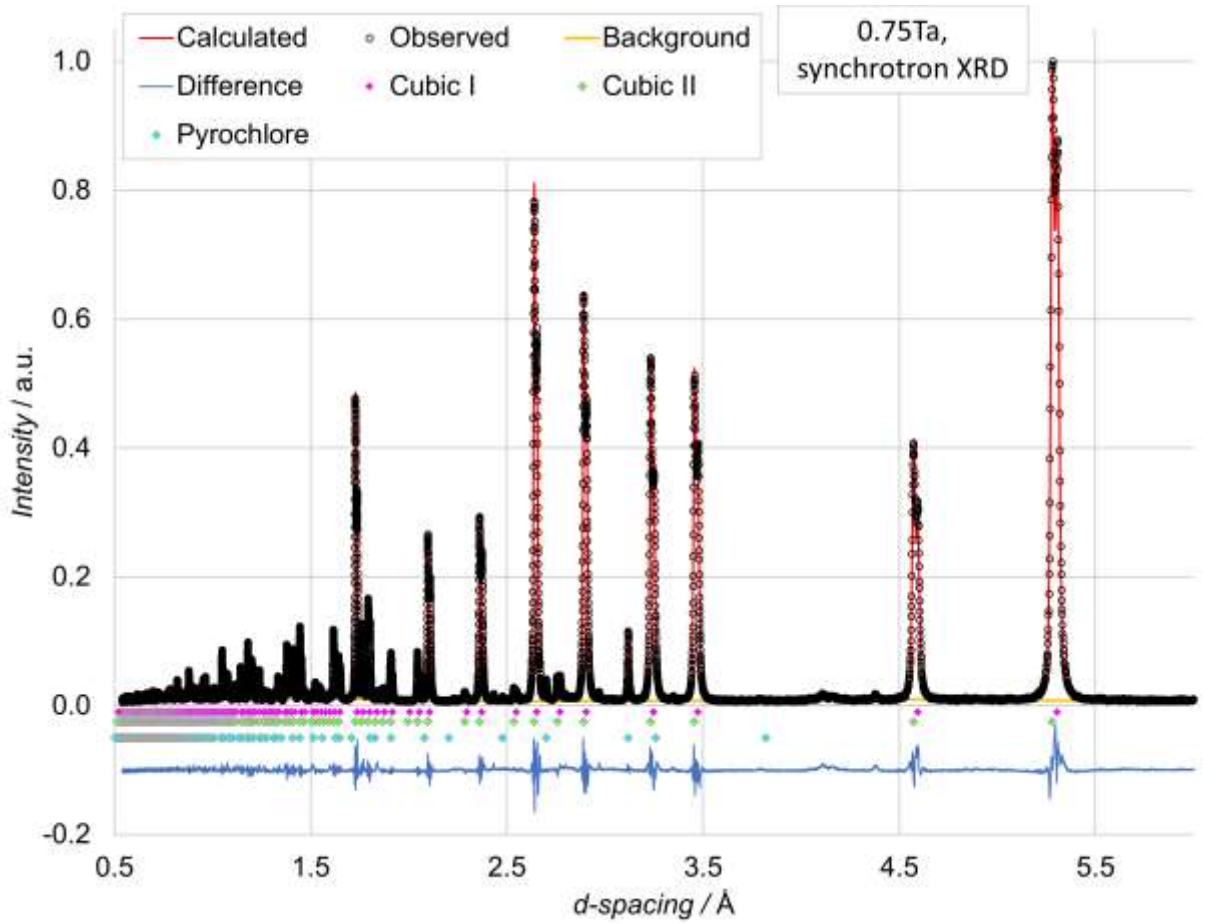

Figure S7. Refinement of synchrotron x-ray diffraction data after convergence for the sample with composition of $Li_{6.25}La_3Zr_{1.25}Ta_{0.75}O_{12}$.

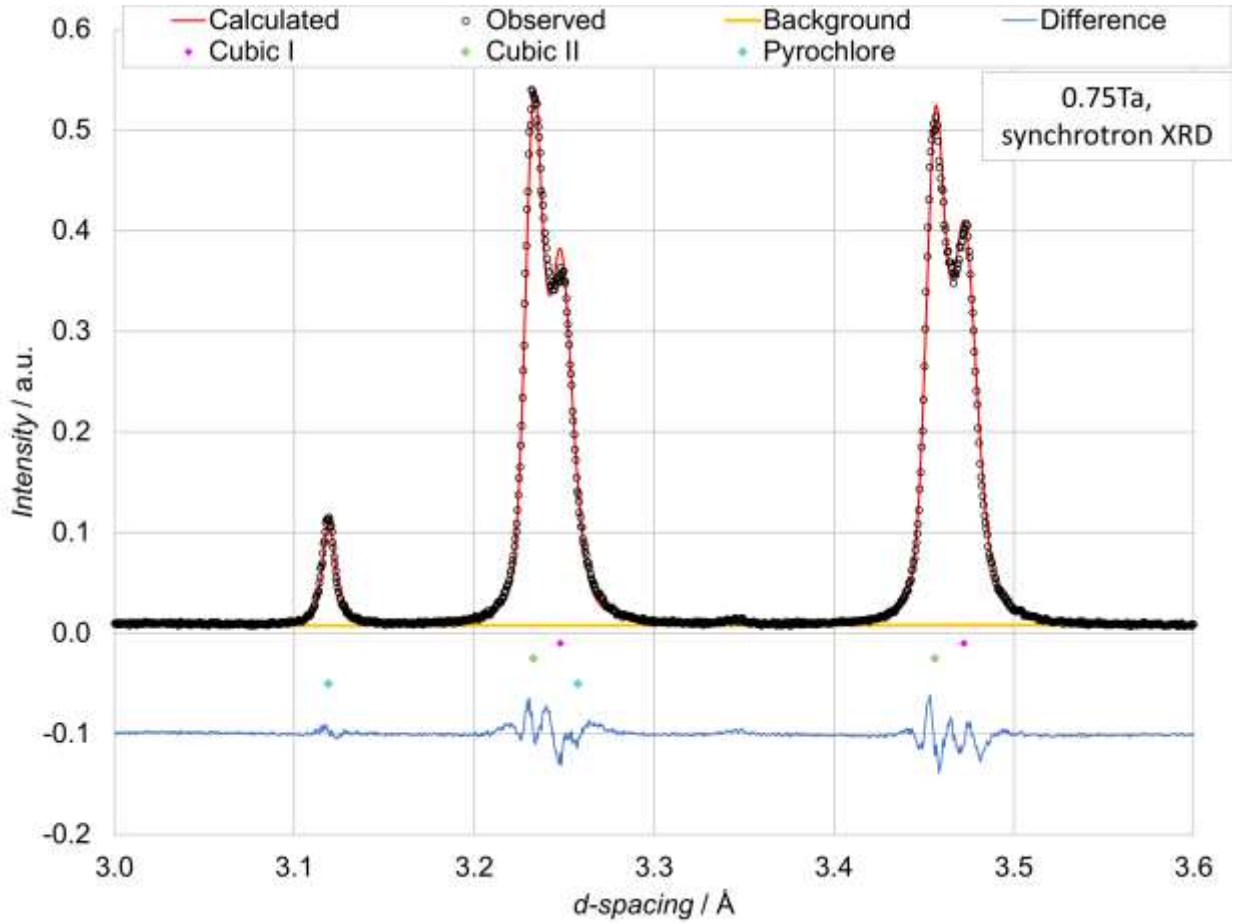

Figure S8. Magnified region of the refinement of synchrotron x-ray diffraction data after convergence for the sample with composition of $Li_{6.25}La_3Zr_{1.25}Ta_{0.75}O_{12}$ highlighting the two cubic phases observed.

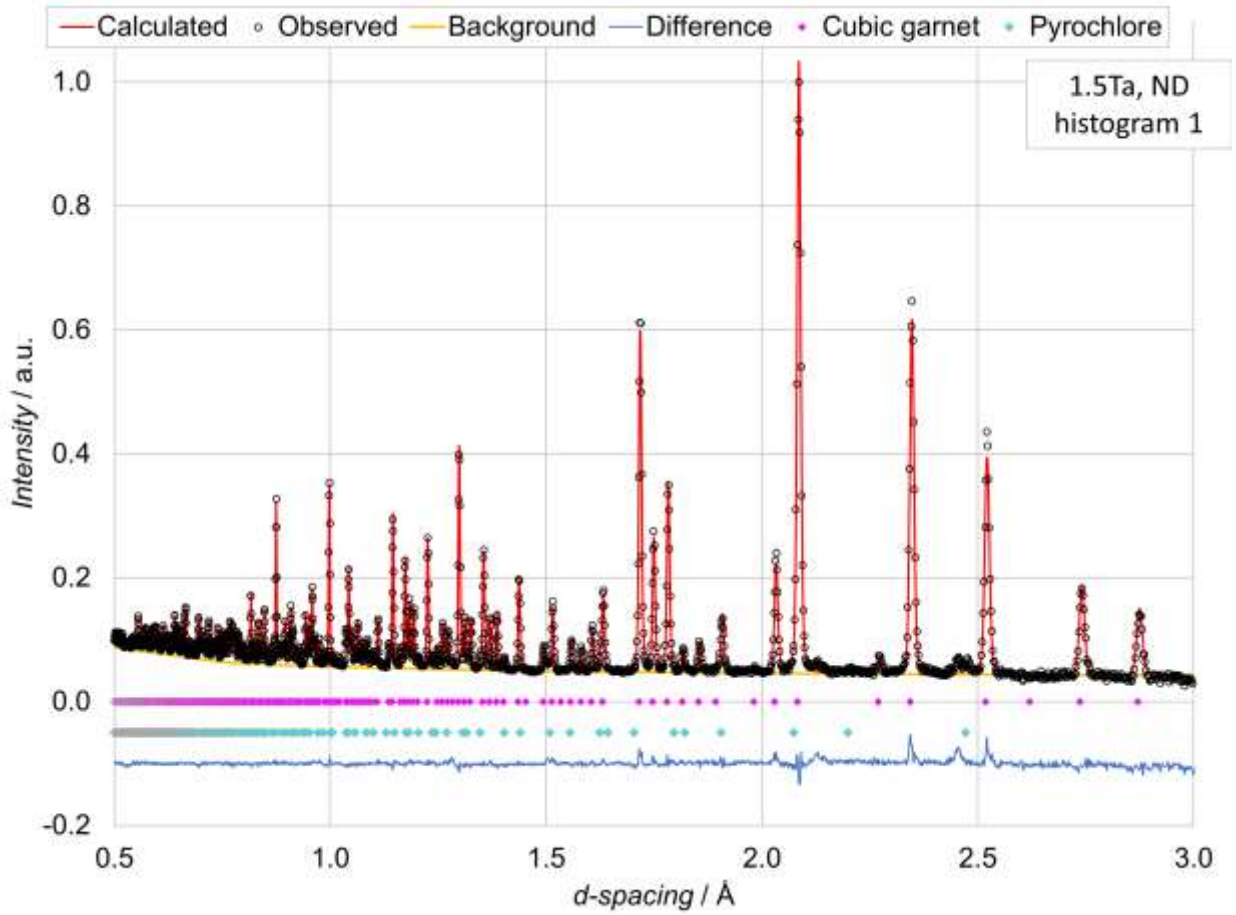

Figure S9. Refinement of neutron diffraction data after convergence for the sample with composition of $Li_{5.5}La_3Zr_{0.5}Ta_{1.5}O_{12}$.

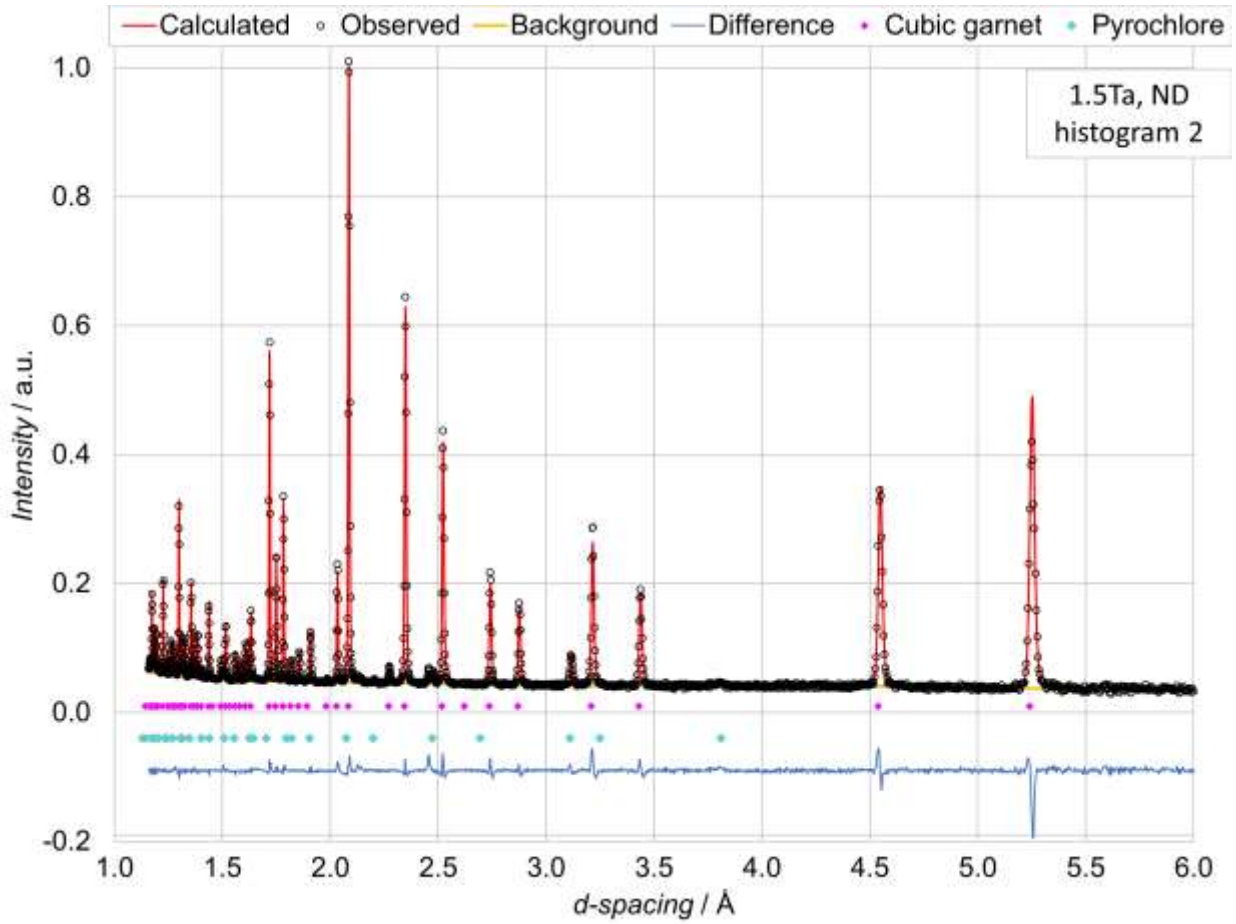

Figure S10. Refinement of neutron diffraction data after convergence for the sample with composition of $Li_{5.5}La_3Zr_{0.5}Ta_{1.5}O_{12}$.

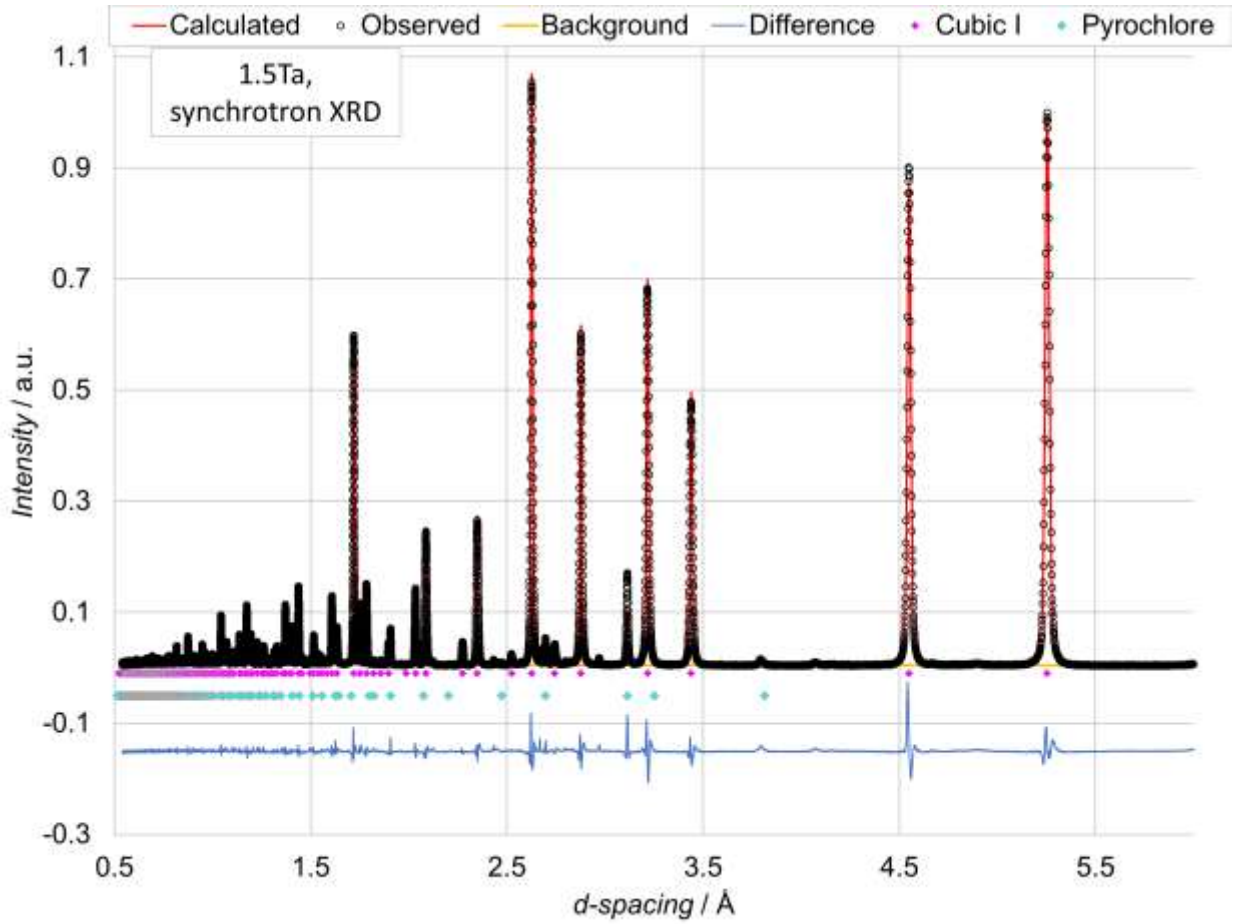

Figure S11. Refinement of synchrotron x-ray diffraction data after convergence for the sample with composition of $Li_{5.5}La_3Zr_{0.5}Ta_{1.5}O_{12}$.

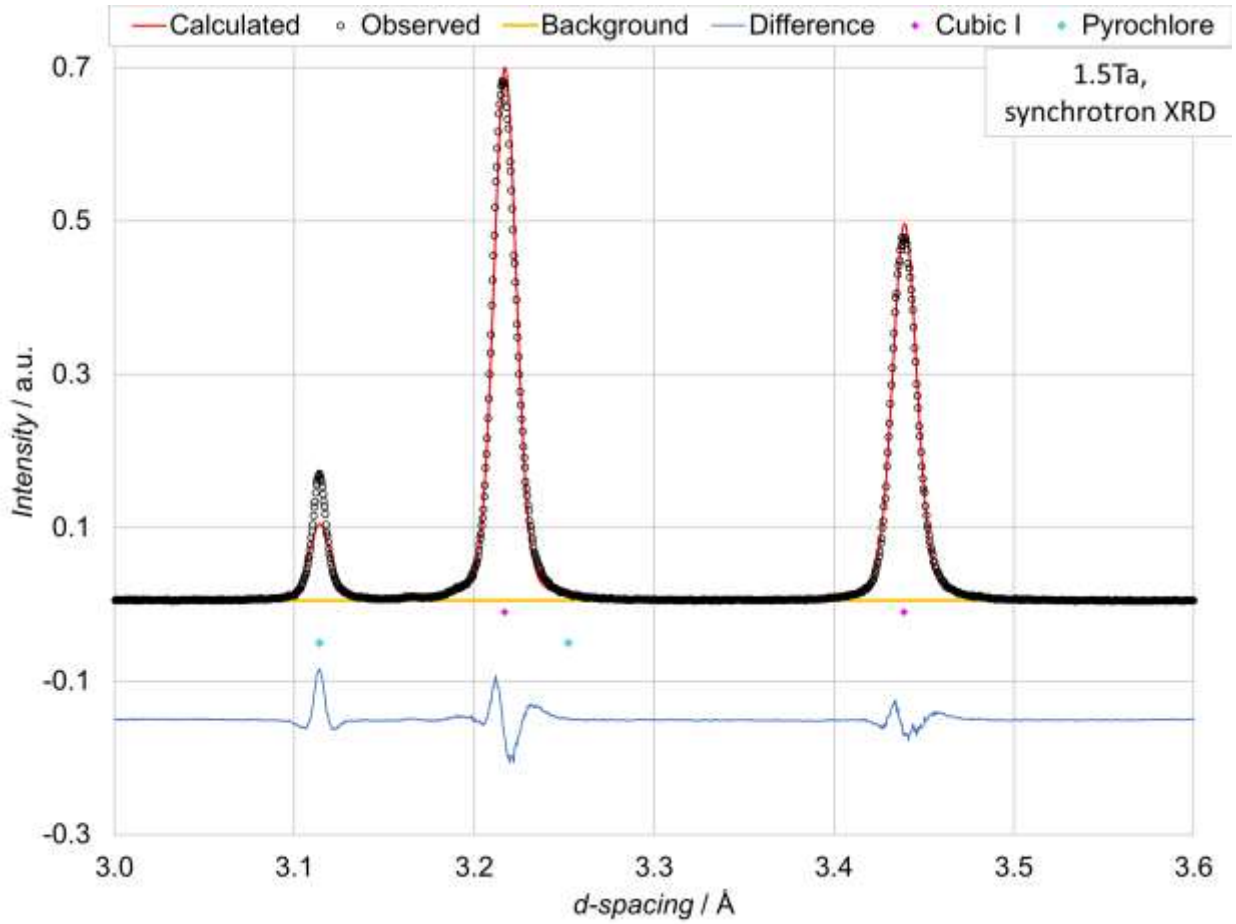

Figure S12. Magnified region of the refinement of synchrotron X-ray diffraction data after convergence for the sample with composition of $Li_{5.5}La_3Zr_{0.5}Ta_{1.5}O_{12}$. Unlike the other compositions, a single cubic phase was observed.

Table S1. Results of the structural refinement for the sample with nominal composition $Li_{6.25}La_3Zr_{1.25}Ta_{0.75}O_{12}$ at 300K.

Name	Site	Site Occupancy	X	Y	Z	$100xU_{eq}$ (Å^2)
Li1	24d	0.450(8)	3/8	0	¼	2.61(13)
Li2	96h	0.354(4)	0.0979(4)	0.6868(4)	0.5785(4)	1.94(11)
La	24c	1.000	1/8	0	¼	0.960(6)
Zr	16a	0.596(2)	0	0	0	0.666(8)
Ta	16a	0.384(2)	0	0	0	0.666(8)
O	96h	1.000	-0.0313(4)	0.0529(5)	0.1481(5)	1.401(6)

Space group Ia-3d (No. 230); a =12.9089(30) Å; R_{wp} = 2.37, χ^2 = 2.996, R_p =4.59

Table S2. Results of the structural refinement for the sample with nominal composition $Li_{5.5}La_3Zr_{0.5}Ta_{1.5}O_{12}$ at 300K.

Name	Site	Site Occupancy	X	Y	Z	$100xU_{eq}$ (Å^2)
Li1	24d	0.646(8)	3/8	0	¼	2.77(10)
Li2	96h	0.262(4)	0.1006(5)	0.6862(5)	0.5781(5)	1.84(14)
La	24c	1.000	1/8	0	1/4	1.030(7)
Zr	16a	0.197(2)	0	0	0	0.552(8)
Ta	16a	0.754(2)	0	0	0	0.552(8)
O	96h	1.000	-0.0302(4)	0.0514(4)	0.1458(4)	1.301(5)

Space group Ia-3d (No. 230); a =12.8363(33) Å; R_{wp} = 2.88, χ^2 = 4.37, R_p = 5.11

Reference

[1] J.TS. Irvine, D.C. Sinclair, A.R. West, *Adv. Mater.* **1990** *2,* 132.

[2] R. A. Huggins, *Ionics* **2002**, *8,* 300.

[3] E. Rangasamy, J. Wolfenstine, J. Sakamoto, *Solid State Ionics* **2012**, 206, 28.

[4] H. Buschmann, J. Dölle, S. Berendts, A. Kuhn, P. Bottke, M. Wilkening, P. Heitjans, A. Senyshyn, H. Ehrenberg, A. Lotnyk, V. Duppel, L. Kienle, J. Janek, *Phys. Chem. Chem. Phys.* **2011**, *13*, 19378.

[5] Li, Y. Cao, X. Guo, *Solid State Ionics* **2013**, *15*, 76.

[6] T. Thompson, J. Wolfenstine, J. L. Allen, M. Johannes, A. Huq, I. N. David, J. Sakamoto, *J. Mater. Chem. A* **2014**, *2*, 13431.

[7] R. Murugan, V. Thangadurai, W. Weppner, *Angew. Chem. Inter. Ed*. **2007**, *46*, 7778.

[8] J. Bisquert, A. Compte, *J. Electroanalytical Chem.* **2001,** *499,* 112.

[9] J. Awaka, A. Takashima, K. Kataoka, N. Kijima, Y. Idemoto, J. Akimoto, *Chem. Lett.* **2011**, *40*, 60.

[10] M. Xu, M. S. Park, J. M. Lee, T. Y. Kim, Y. S. Park, E. Ma, *Phys. Rev. B* **2012,** *85,* 052301.

[11] A. Logéat, T. Köhler, U. Eisele, B. Stiaszny, A. Harzer, M. Tovar, A. Senyshyn, H. Ehrenberg, B. Kozinsky, *Solid State Ionics* **2012**, *206*, 33.

[12] D. Rettenwander, C. A. Geiger, G. Amthauer, *Inorg. Chem.* **2013**, *52*, 8005.

[13] C.A. Geiger, E. Alekseev, B. Lazic, M. Fisch, T. Armbruster, R. Langner, M. Fechtelkord, N. Kim, T. Pettke, W. Weppner, *Inorg. Chem.* **2011**, *50*, 1089.

[14] A.A. Hubaud, D.J. Schroeder, B. Key, B.J. Ingram, F. Dogan, J.T. Vaughey, *J. Mater. Chem. A* **2013,** *1*, 8813.